Journal of Colloid and Interface Science 576 (2020) 147–157

Contents lists available at ScienceDirect

Journal of Colloid and Interface Science

journal homepage: www.elsevier.com/locate/jcis

Grafted nanocellulose and alkaline nanoparticles for the strengthening and deacidification of cellulosic artworks

Q. Xu, G. Poggi *, C. Resta, M. Baglioni [1], P. Baglioni *,[1]

CSGI and Chemistry Department, University of Florence, Via della Lastruccia 3, 50019 Sesto Fiorentino, FI, Italy

GRAPHICAL ABSTRACT

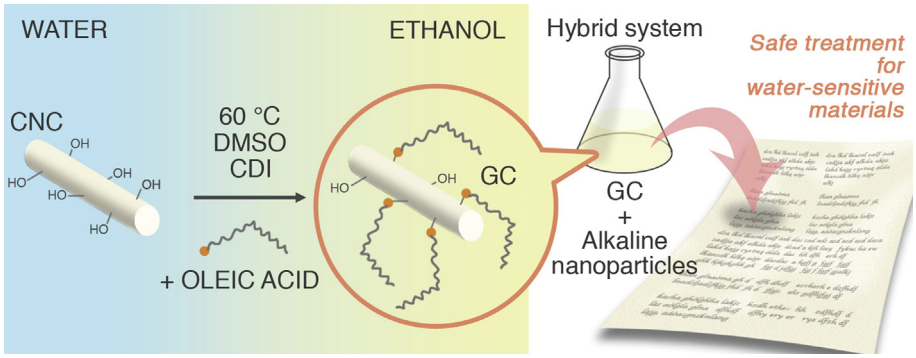

ARTICLE INFO

Article history:
Received 25 March 2020
Revised 4 May 2020
Accepted 5 May 2020
Available online 6 May 2020

Keywords:
Nanocellulose
Grafting
Alkaline nanoparticles
Deacidification
Strengthening
Paper
Calcium carbonate
Calcium hydroxide
Cultural heritage conservation

ABSTRACT

Hypothesis: Strongly degraded cellulosic artworks usually need deacidification and consolidation. Alkaline nanoparticles are known to be effective in neutralizing the acidity, while cellulose nanocrystals have the potential to be used as compatible and effective strengthening agents.
Experiments: We have grafted cellulose nanocrystals with oleic acid using a 1′1-carbonyldiimidazole-mediated procedure, to increase their dispersibility in organic solvents, and synthesized $Ca(OH)_2$ or $CaCO_3$ nanoparticles via a solvothermal process. Grafted nanocellulose and alkaline nanoparticles were used to prepare ethanol-based "hybrids". Prior to the application, the physico-chemical properties of nanocellulose dispersions and "hybrids" were studied by rheology and small-angle X-ray scattering.
Findings: Cellulose nanocrystals were effectively grafted and stably dispersed in ethanol. It was shown that the use of ethanol as a dispersing medium, and the addition of alkaline nanoparticles act in a synergistic way, increasing the interactions between grafted cellulose nanocrystals, leading to the formation of clusters. These dispersions are thixotropic, a behavior particularly appealing to conservation purposes, since they can be applied in the liquid state, or, when a more confined application is required, they can be applied in a gel-like state. As a result of the application, an improvement in the mechanical properties of paper and an increase of pH were obtained.

1. Introduction

Cellulose-based materials, such as paper, canvas and wood, constitute a large part of the global patrimony of humankind. A significant amount of documentary, historical and artistic materials is in

* Corresponding authors.
E-mail addresses: poggi@csgi.unifi.it (G. Poggi), baglioni@csgi.unifi.it (P. Baglioni).
[1] No kinship exists among these authors.

https://doi.org/10.1016/j.jcis.2020.05.018
0021-9797/

the need of urgent intervention due to their poor conservation conditions [1].

The most important degradation mechanism of cellulose-based artifacts is the acid-catalyzed hydrolysis of the β-1,4-glycosidic bonds, which causes a decrease of the polymerization degree (DP) and a substantial loss in the original mechanical properties [2–4]. Recently, NMR diffusometry and relaxometry have been used to gather new insights about the changes in the network of cellulose after acid-catalyzed hydrolysis, showing an enlargement of the macropore structure of paper that can, in turn, favor the penetration of pollutants from the atmosphere, enhancing the acidification process itself [5,6]. Compounds from the making process, original components, or even materials used in past conservation treatments are acidic or may develop acidic products upon aging, triggering the degradation process of cellulose-based artworks.

Over the last twenty years, we have developed an approach based on the use of colloidal systems for the conservation of cultural heritage [7–11]. Alkaline nanoparticles, such as calcium or magnesium hydroxide dispersed in short-chain alcohols, were proposed as an effective tool for the deacidification of paper and canvas in the early 2000s [12]. Calcium and magnesium hydroxide nanoparticles have been applied for the deacidification of waterlogged wood [13–15], wood from organ pipes [16], paper and canvas [12,17–21], and underwent extensive assessment with excellent results [22–24]. However, when the mechanical properties of cellulose-based artifacts are lost upon aging, a reinforcement is needed, in addition to a deacidification process. For instance, a relining can be carried out on canvases [25], while the mending using Japanese paper and adhesives is usually selected for paper [26].

Nanocellulose has recently gathered attention due to its unique features that can be of interest in several applicative fields. In fact, nanocellulose is non-toxic, renewable, biodegradable and forms almost transparent films [27,28]. The term "nanocellulose" refers to cellulose nanocrystals (CNC) and to cellulose nanofibrils (CNF) [27,28]. CNC are usually extracted from cellulose by a heavy acid treatment [29]. They are rod-shaped, highly crystalline nanoparticles with high mechanical properties and surface area [27,28], and, thus, they have been used as reinforcing agents of synthetic polymers [30], as paper coatings [31], or added to paper pulp before sheet formation [32,33]. These materials, which are thoroughly compatible with cellulose-based works of art, have been recently proposed as consolidants for canvases [34–36] and as adhesives for paper mending [37].

However, acidic and strongly degraded cellulosic works of art usually require both deacidification, to hinder further cellulose depolymerization, and a consolidation treatment to improve their mechanical strength. Aged artifacts are usually very fragile and the application of the two separated conservaton procedures should be avoided to reduce the risks and the stresses for the original materials, which are always connected to a conservation intervention. A single-step treatment is therefore to be preferred, especially in the case of degraded works of art.

Degraded cellulose-based artworks usually cannot withstand the application of water-based treatments. Here we report on the preparation of ethanol-based "hybrid" systems and on CNC's surface modification with oleic acid to allow the preparation of stable dispersions of cellulose nanocrystals in ethanol. The obtained CNC were characterized using Attenuated Total Reflection Fourier-Transform Infrared Spectroscopy (ATR-FTIR), Thermogravimetric analysis (TGA) and Atomic Force Microscopy (AFM). The final systems for the concomitant strengthening and deacidification are composed of grafted nanocellulose and alkaline nanoparticles, and were characterized using rheology and Small-Angle X-ray Scattering (SAXS). The efficacy of the proposed system for the reinforcement and deacidification of acidic paper was evaluated from tensile strength, pH and colorimetric measurements.

2. Materials and methods

2.1. Materials

Dimethyl sulfoxide (DMSO, anhydrous 99.9%), 1′1-carbonyldiimidazole (CDI, reagent grade) and oleic acid (90%) were purchased from Sigma-Aldrich. These reagents were used for the surface modification of cellulose nanocrystals. Cellulose nanocrystals (0.7–0.8% of residual sulfur) are from CelluForce, Canada. Sulfuric acid (96%, Carlo Erba) was used for the acidification of paper. All reagents were used as received without further purification. Highly pure water (having a resistivity of 18 MΩ cm) produced by a Millipore Milli-Q UV system and ethanol (absolute, Fluka, 99.9%) were used during the experiments.

2.2. Oleic acid-grafted cellulose nanocrystals (GC) synthesis

The oleic acid-grafted cellulose nanocrystals (GC) synthesis was based on a 1′1-carbonyldiimidazole (CDI)-mediated method, developed by Hussain and Peng, to obtain grafted crystals with a DS ≈ 0.26 [38,39]. When required, reaction operations were carried out under inert atmosphere, according to the standard Schlenk technique, employing dried and purified nitrogen. A mixture of CNC (0.50 g) and 12 mL of DMSO was magnetically stirred for 30 min and then sonicated for 2 min with a Branson S-450 ultrasonifier equipped with a micro-tip, until an almost completely transparent dispersion was obtained. CDI (0.67 g, 4 mmol) was dissolved in 12 mL of dry DMSO and treated with 1.16 g (4 mmol, 1 eq.) of oleic acid. The solution was stirred for 1 h at 60 °C and then the dispersion of CNC in DMSO was added. The reaction temperature was raised up to 80 °C and the system was kept under stirring for 24 h. The mixture was then cooled down to room temperature and the particles were precipitated by addition of water (about 150 mL), recovered by centrifugation and washed twice with ethanol (around 100 mL in total). The product was collected by centrifugation and stored as an ethanol suspension (about 35–40 g/L).

2.3. Alkaline nanoparticles synthesis

Calcium hydroxide and calcium carbonate nanoparticles were prepared using a solvothermal synthesis, starting from ethanol and calcium metal, according to the following scheme [15]:

$$Ca + 2\,C_2H_5OH \rightarrow Ca(C_2H_5O)_2 + H_2 \quad (1)$$

$$Ca(C_2H_5O)_2 + 2\,H_2O \rightarrow Ca(OH)_2 + 2\,C_2H_5OH \quad (2a)$$

$$Ca(C_2H_5O)_2 + 2\,H_2O + CH_3CH_2{-}(CO_3){-}CH_2CH_3 \rightarrow CaCO_3 + 4\,C_2H_5OH \quad (2b)$$

More in details: 10 g of granular calcium and 500 mL of ethanol were placed inside a high-pressure reactor (Parr-instruments). Vacuum/nitrogen cycles were performed before the reaction to ensure an oxygen-free atmosphere inside the reaction chamber. During the first step of the reaction, calcium alkoxide was obtained (1). To hydrolyze calcium alkoxide to calcium hydroxide, 35 mL of water was added inside the reaction chamber by means of a steel pipette in a nitrogen atmosphere (2a). Alternatively, to hydrolyze the alkoxide to calcium carbonate, 35 mL of water and 35 mL of diethyl carbonate were added (2b). The addition was carried out at 70 °C and the system was stirred for 60 min.

Calcium hydroxide nanoparticles are hexagonal platelets with a high degree of ordering, having a thickness of about 20–30 nm and an average diameter (obtained by laser diffraction) of about 140 nm, while calcium carbonate nanoparticles have a volume-

based size distribution centered at about 70 nm, and are mainly composed of vaterite and calcite.

2.4. CNC and GC characterization

The FT-IR spectra of GC, CNC, oleic acid and DMSO were recorded using a Thermo-Nicolet Nexus 870 spectrometer equipped with a liquid nitrogen-cooled Mercury Cadmium Telluride detector and a single reflection diamond crystal ATR unit. The spectra were obtained from 128 scans with 2 cm^{-1} of optical resolution, in the 4000–650 cm^{-1} range.

The thermal behavior of GC, CNC, and oleic acid was determined by differential thermogravimetry (DTG) using an SDT Q600 TA Instrument, operating between 30 and 500 °C at a heating rate of 10 °C/min under nitrogen flow (100 mL/min). For each measurement, about 30 mg of sample was placed inside an aluminum pan and analyzed. From the thermal curves, the pyrolysis temperature (Tp), defined as the maximum of the weight loss derivative, was recorded and used to gain information about the composition of the sample. Tp experimental error was ±1 °C.

Atomic force microscopy (AFM) images were collected on CNC and GC particles with a XE7 system (Park System Corp., Korea). The images were acquired in non-contact mode using SSS-NCHR 10M AFM tips with a radius of curvature < 5 nm, a nominal force constant of 42 N m^{-1}, and a resonance frequency of 272 kHz (drive = 66%). Samples were prepared by placing about 10 μL of CNC in water and GC in ethanol (about 3 mg/L) over a freshly cleaved mica sheet and allowing them to rapidly evaporate.

2.5. CNC, GC dispersion and "hybrid" systems preparation

CNC aqueous dispersions were prepared starting from CNC dried powder, which was dispersed in water by stirring for 6 h at 800 rpm and subsequently sonicated for 5 min with a Branson S-450 (450 W) equipped with a micro-tip. For the preparation of CNC dispersions in water/ethanol mixtures, ethanol was gradually added to a highly-concentrated aqueous CNC dispersion kept under stirring.

30 g/L GC dispersions were prepared by diluting concentrated GC (as obtained from the synthetic procedure) with ethanol. Dispersions were stirred for 4 h at 800 rpm and then sonicated for 5 min with a Branson S-450 ultrasonifier (450 W) equipped with a micro-tip.

For the preparation of "hybrid" systems, alkaline nanoparticles were added to the GC dispersions, which were immediately mixed with a vortexer. After some preliminary tests, two different alkaline nanoparticles concentrations in the CNC "hybrids", namely, 0.7 g/L and 3 g/L, were used for the preparation of the final systems. Name and composition of the prepared systems are reported in Table 1.

2.6. GC and "hybrids" characterization

Considering that the viscoelastic properties of samples were changing with time, a characterization on freshly prepared samples left undisturbed for variable number of days to clarify the aging effect on these properties was performed. Rheological measurements were carried out with a TA Instrument Hybrid Rheometer DISCOVERY HR-3, using a plate-plate geometry (flat plate 40 mm diameter) and a Peltier for temperature control. The cell was closed by lowering the head to the measuring position in the axial force-controlled mode. Each sample was gently loaded onto the plate and care was taken to minimize the stress to the sample during the loading procedure. Silicone oil was used to minimize the evaporation of ethanol during tests. Measurements were performed at 25 °C, with a 600 s soak time and at least twice on duplicate samples. Amplitude sweep tests (γ = 0.01–100%; 1 Hz) were performed to determine the linear viscoelastic region (LVE). Frequency sweep measurements were carried out over the frequency range 0.1–50 Hz at a constant strain of 0.2%, within LVE domain. Three interval thixotropy tests (3ITT) were performed as follows: after 600 s of soak time to remove the eventual loading effects, a first step of 90 s was performed within the linear viscoelastic range (γ = 0.02%). In the second interval, after a soak time of 60 s, a large amplitude oscillatory strain was applied (γ = 80%) for 90 s with the aim of breaking down the structure of the system. In the third interval, after 600 s of soak time, a third test was conducted with the same conditions used in the first interval, so to favor the recovery of the internal structure.

Small-angle X-ray scattering (SAXS) measurements were performed with a HECUS S3-MICRO SWAXS-camera, equipped with a Hecus System 3 2D-point collimator (min divergence 0.4 × 0.9 $mrad^2$) and two position sensitive detectors (PSD-50 M) consisting of 1024 channels with a width of 54 μm. During the experiments, the K_α radiation (λ = 1.542 Å) emitted by a Cu anode from the Oxford 50 W microfocus source with customized FOX-3D single-bounce multilayer point focusing optics (Xenocs, Grenoble) was used, while the K_β line was removed by a multilayer filter. The voltage was generated by the GeniX system (Xenocs, Grenoble). The sample-to-detector distance was 26.9 cm. The volume between the sample and the detector was kept under vacuum during the measurements to minimize the scattering from the atmosphere. The camera was calibrated in the small-angle region using silver behenate (d = 58.38 Å). Scattering curves were obtained in the q-range between 0.01 and 0.6 $Å^{-1}$ at 25 °C. Samples were placed in 1.5 mm thick quartz capillary tubes sealed with hot-melting glue.

Table1
Nomenclature and composition of oleic acid-grafted cellulose nanocrystals dispersions, GC, and "hybrid" systems.

GC dispersions and "hybrid" systems nomenclature		
Name	NanoP type	NanoP g/L
GC	–	–
GC-OH.7	$Ca(OH)_2$	0.7
GC-OH3		3
GC-CO.7	$CaCO_3$	0.7
GC-CO3		3

2.7. Application to paper

Filter paper (qualitative grade from cotton linters, paper grammage 75 g/m^2, Munktell) was used to test the efficacy of the "hybrid" systems. Paper sheets were immersed in a sulfuric acid solution (pH = 2.5) for 30 s and aged for 20 days at high temperature and relative humidity (80 °C and 75% RH). These aged paper samples are labelled as AP. Unaged filter paper, labelled as P, was characterized and used as a reference system.

Three treatments were selected to be tested, namely GC, GC-OH3 and GC-CO3. All the treatments were applied by brush on both sides of paper samples measuring 6 × 8 cm^2. Samples were left to dry for at least two days before testing. Samples treated with calcium hydroxide nanoparticles were stored at 50% RH for 14 days, to allow the full conversion of calcium hydroxide excess into carbonate. Samples were weighed before and after the application. The samples weight change due to the application was about 10%, which corresponds to a surface coverage on paper of about 7.5 g/m^2.

2.8. Characterization of paper

The pH of paper was measured using the following protocol: 125 mg of sample was weighed, cut in small pieces, and placed

inside screw top vials. 9 mL of distilled water was added inside each vial, subsequently sealed to avoid the solubilization of CO_2 from air into water. Vials were kept under stirring for one hour before measuring the pH of the extraction by using a digital pH-meter (CrisonBasic 20, equipped with a combined electrode, model 52–21). Three measurements were performed on each sample. The error associated to pH measurements on these samples is ±0.2.

A X-RITE SP60 VIS portable spectrophotometer, with an integrating sphere having a circular sampling spot (diameter = 1.5 cm) was used to analyze the samples. Colorimetric coordinates were obtained using standard illuminant D65 and a standard observer at 2°. The color difference between samples can be expressed in terms of the ΔE parameter, calculated from the colorimetric coordinates and L*, a*, and b* as follows:[40]

$$\Delta E = \sqrt{\left(L_2^* - L_1^*\right)^2 + \left(a_2^* - a_1^*\right)^2 + \left(b_2^* - b_1^*\right)^2}$$

The experimental error of colorimetric measurements on paper is ±0.75.

The Yellowness Index (YI), which describes the change in color of a test sample from clear or white to yellow, was calculated as indicated in the ASTM E313 standard [41]. The experimental error of YI is ±1.

Tensile strength measurements were conducted on paper stripes using a TA Instrument Hybrid Rheometer DISCOVERY HR-3, equipped with a Film Tension Dynamic Mechanical Analysis tool. As in a standard tensile test, the sample is held in position by two clamps placed at a fixed distance and then pulled at a preset rate. The instrument records the elongation and the force that pulls the upper moving jaw away from the lower stationary one. Before the test, the specimens were conditioned at 50% RH and 23 °C for at least 24 h. Each stripe (1 × 8 cm^2) was clamped on two jaws, whose distance was fixed at 4 cm. The rate of separation of the two jaws was set at 94 μm/s. The rate of grip separation was reduced with respect to standards [42,43] in proportion to the reduction in effective specimen length, so that sample rapture takes place between 10 and 30 s, as indicated in the ASTM standard [42]. Six measurements were performed for each series of samples. The mean value of the load at which sample rapture occurred was used to calculate the Ultimate Tensile Strength (UTS), given by:

$$UTS = AF/W \ [kN/m]$$

where AF is the axial force at rupture and W is the width of the sample, measured with a digital caliper.

3. Results and discussion

3.1. Cellulose nanoparticles characterization

Water, which is commonly used in conservation practice, can solubilize compounds in paper sheets such as sizing agents, writing fluids, inks or dyes [44], and can swell cellulose fibers, leading to a decrease in the mechanical properties and changes in sheet texture [45,46]. Therefore, the use of water-based treatments is often discouraged, particularly in case of ancient artifacts/documents. In order to get an active material fully dispersible in neat organic solvents, we modified the surface of cellulose nanocrystals with oleic acid by CDI-mediated esterification of the –OH moieties of cellulose.

Fig. 1A shows the ATR-FTIR spectra of GC (black), CNC (green), oleic acid (blue) and DMSO (red). The spectra of GC and CNC were normalized using the C—C vibration at 1060 cm^{-1}. The spectrum of GC shows clear evidence that the esterification reaction occurred. As shown in the inset (1), the oleic acid C=O stretch band was shifted from 1711 cm^{-1} to 1735 cm^{-1}, indicating the formation of an ester group [47]. Moreover, in the 2850–2950 cm^{-1} range, two sharp peaks at 2921 and 2856 cm^{-1} are visible in the GC spectrum, while only one broader and less defined band can be found in the same range of the CNC spectrum. These two peaks can be assigned to the asymmetric and symmetric CH_2 stretch, arising from the aliphatic chain of the oleate moieties [48]. No peaks of DMSO, which is the reaction solvent, can be found in the ATR spectrum of GC. These results clearly show that oleic acid was successfully grafted on CNC, and no reactants or side compounds are found in the reaction products.

Thermal analyses of GC, CNC and oleic acid revealed different degradation profiles (Fig. 1B). The initial small weight loss of CNC and GC in the temperature range 50–100 °C can be ascribed to the evaporation of physically bound moisture. The sharp peak in the CNC thermal curve, corresponding to the degradation of cellulose nanocrystals, is located at about 300 °C, similarly to what has been reported by Johar [49]. On the contrary, the main degradation peak of the GC sample is a broad signal located in the 200–400 °C range having a maximum at 280 °C. The lower thermal stability of GC can be ascribed to the surface grafting. In fact, oleic acid degrades at about 250 °C and the presence of oleate moieties on the surface of nanocrystals is responsible for both the decrease in the pyrolysis temperature and the broadening of the peak.

The effective surface modification of cellulose nanocrystals is confirmed by the AFM pictures reported in Fig. 1C/F. Cellulose nanocrystals produced by sulfuric acid hydrolysis of cellulose usually yield negatively charged CNC particles and are poorly prone to interact with the negatively charge mica surface. However, thanks to the grafting, GC deposit on the freshly cleaved mica surface more easily than CNC, and are prone to form clusters.

3.2. GC and "hybrid" systems characterization

The mechanical response of GC systems in the presence of nanoparticles, "hybrid" systems, was assessed using frequency sweep measurements and compared to CNC in water, CNC in a water/ethanol blend (50 wt%), and GC in ethanol. CNC dispersed in aqueous solutions with more than 50% of ethanol tend to flocculate and aggregate, resulting in unstable dispersions.

The mechanical dynamic response exhibited by CNC in water (light green markers in Fig. 2A), is characteristic of a viscoelastic liquid, i.e. of an entangled system where nanocrystals interactions are negligible: at low frequencies the system behaves as a diluted solution (predominant viscous behavior, G" > G'), while at high frequencies the response becomes more solid-like (G' ≈ G"), as the system cannot rearrange within the time of an oscillation [50]. On the other hand, CNC in a water/ethanol blend display a solid-like mechanical spectrum, being G' ≫ G" over the entire range of investigated frequencies, with both moduli almost frequency-independent (see dark green markers in Fig. 2A). Moreover, G' and G" are more than 10 times higher than in the water-based dispersion. In Fig. 2B, the response of GC is reported: here G' is significantly higher than G" over the investigated range of frequency and both moduli are almost completely frequency-independent, as typical of gel-like systems. Moreover, G' and G" are several orders of magnitude higher than CNC in water and more than ten times higher than CNC in the water/ethanol blend. CNC produced by sulfuric acid hydrolysis of cellulose usually yield negatively charged particles with surface sulfate groups [51]. The difference in the mechanical response of the three dispersions reported in Fig. 2A/B, i.e., CNC in water, CNC in water/ethanol, and GC in ethanol, can be related to a change of the dielectric constant of the two solvents (permittivity of ethanol is lower than water, i.e. 24.5 and 78, respectively) affecting the Debye length and to the presence of oleic moieties on GC surface. This results, in turn, in an increase of the interactions between crystals and, thus, in systems with a stronger solid-like behavior.

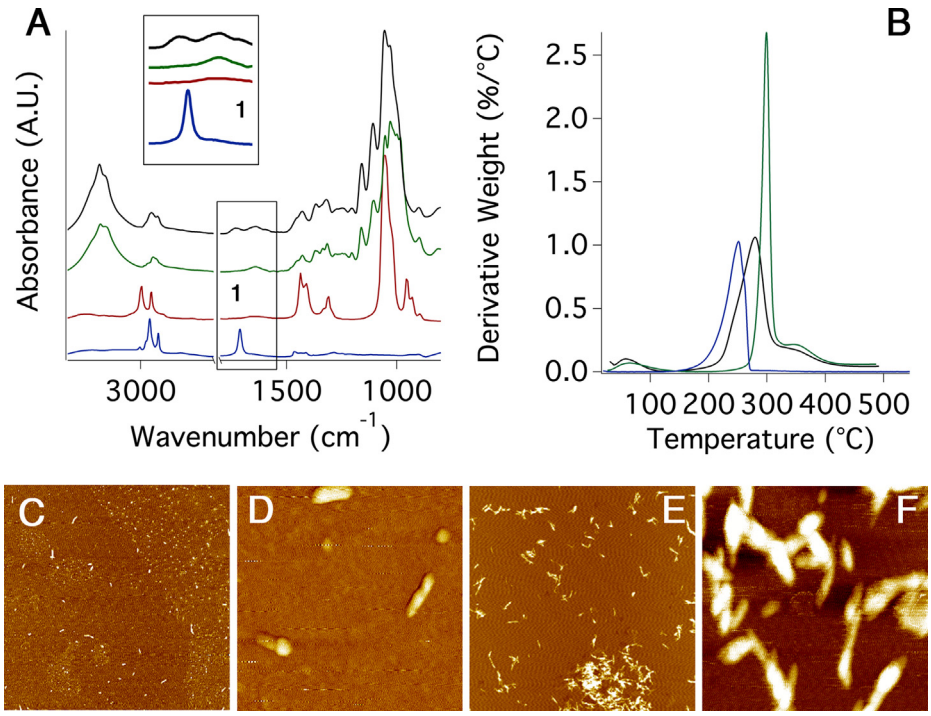

Fig. 1. (A) ATR-FTIR spectrum of oleic acid (blue), DMSO (red), CNC (green) and GC (black). (B) DTG curves of oleic acid (blue), CNC (green) and GC (black). (C-D) AFM pictures of CNC over a fleshly cleaved mica sheet (10×10 μm^2 and 1×1 μm^2, respectively). (E-F) AFM picture of GC over a fleshly cleaved mica sheet (10×10 μm^2 and 1×1 μm^2, respectively). (For interpretation of the references to colour in this figure legend, the reader is referred to the web version of this article.)

Rheological measurements were also carried out on "hybrid" systems having different concentrations of alkaline nanoparticles. The addition of $Ca(OH)_2$ nanoparticles (0.7 g/L) leads to a strong increase in G' and G", more than 10 times higher than in GC (light red markers in Fig. 2C). Moreover an increase in the alkaline nanoparticles concentration (3 g/L, dark red markers in Fig. 2C) leads to further increase in the gel-like character (higher G' and G") of the systems. It has been recently shown that the addition of divalent ions, such as Ca^{2+} to charged nanocelluloses can induce the gelation of aqueous dispersion by screening the repulsive forces generated by surface charges [52,53]. As distances between crystals are reduced during gelation, divalent ions may interact with different crystals, increasing the mechanical strength of the system [52]. The addition of $CaCO_3$ nanoparticles leads to a small change in the mechanical spectrum of the systems, even though both G' and G" are higher than those of GC, depending on the final concentration of alkaline nanoparticles in the systems (see Fig. 2D). This phenomenon can be explained by the lower water solubility of calcium carbonate, with respect to calcium hydroxide, which leads to a less pronounced effect on the screening of the repulsive forces between crystals.

Figs. 2B, 3A and B show the changes in the rheological spectrum of GC, GC-OH3 and GC-CO3, respectively, as a function of time. Regardless of the time, the G' and G" curves of GC are almost superimposed, indicating that the equilibrium is reached after 24 h from the preparation (see Fig. 2B). On the other hand, the moduli values of "hybrids" increase with increasing time, up to 7 days, when a stabilization finally occurred. The fact that "hybrids" require more time to reach the equilibrium can be ascribed both to the high viscosity of the systems, which partially hampers the rearrangement of cellulose nanocrystals after the addition of alkaline nanoparticles, and to the slow solubilization of alkaline nanoparticles in the dispersing medium, which contains only traces of water.

For all the systems tan δ, which is the averaged G"/G' over the frequency range investigated, was calculated; the obtained values are reported in Table 2. Tan δ has been used to differentiate gel-like systems in two categories, namely, "weak" and "strong". Systems having a tan $\delta > 0.1$ are considered weak gels. On the contrary, a tan $\delta < 0.1$ is typical of strong gels [50,54,55]. Interestingly, after 1 day from the preparation, all the dispersions can be clearly considered weak gels, except for GC-OH3, whose tan $\delta = 0.1$ is in the limit of the strong gel range. After 7 days, also the system containing 0.7 g/L of $Ca(OH)_2$ nanoparticles reached the threshold value and behaved as a strong gel. Therefore, even from the standpoint of tan δ, the "hybrids" with calcium hydroxide nanoparticles can be considered stronger systems, showing a solid-like behavior, indicating the presence of attractive interaction among GC units and a role of Ca^{2+} in the screening of repulsive forces between cellulose nanocrystals.

After 7 days from the preparation, three-interval thixotropy tests (3ITT), which are used to evaluate the deformation and recovery of the structure [56–58], were performed on GC, GC-OH3 and GC-CO3 (see Fig. 4). The measurement is composed of three testing intervals: a low-strain interval, to be used as a reference of an undisturbed material; a high-strain interval, to break the internal structure; a final stage at low-strain conditions to favor the regeneration of the structure. In the first interval, all the systems maintained their original structure under a 0.2% strain. During the second step, after the application of a high strain, the systems behaved as liquids (G" > G'). In the third interval, the same conditions of the first interval were applied resulting in an almost complete recovery of the initial gel-like character [59]. From an applicative point of view, this behavior represents an interesting and important feature. In fact, these systems can be applied either in the liquid or in the gel state. They can be used as liquids, after being energetically shaken. Conversely, when a more confined application is required, they can be applied, with a gentle action, in gel-like state, as the one shown in Fig. 4D/F. Here all the systems, after being energetically shaken, were applied by brush to allow for a proper comparison of their effectiveness.

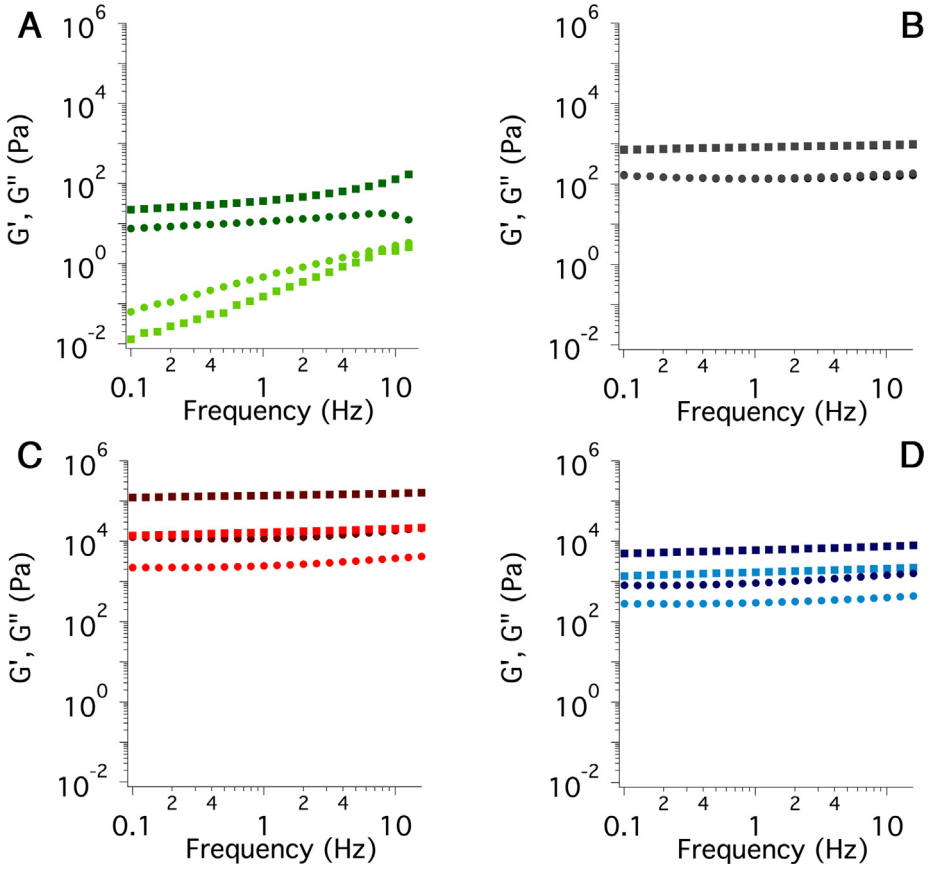

Fig. 2. Frequency sweep measurements of systems with CNC and GC - G'(■), G"(●). Error bars are included in the dimensions of the markers. Measurements were repeated at least twice on duplicate samples. (A) CNC in water (light green) and in a water/ethanol blend (50 wt%) (dark green). (B) GC in ethanol after 1 day (gray) and after 7 day (black) from the preparation. Please note that the data are superimposed. (C) "hybrid" systems with calcium hydroxide nanoparticles: GC-OH.7 (light red, 0.7 g/L) and GC-OH3 (dark red, 3 g/L). (D) "hybrid" systems with calcium carbonate nanoparticles: GC-CO.7 (light blue, 0.7 g/L) and GC-CO3 (dark blue, 3 g/L). Error bars are included in the dimensions of the markers. (For interpretation of the references to colour in this figure legend, the reader is referred to the web version of this article.)

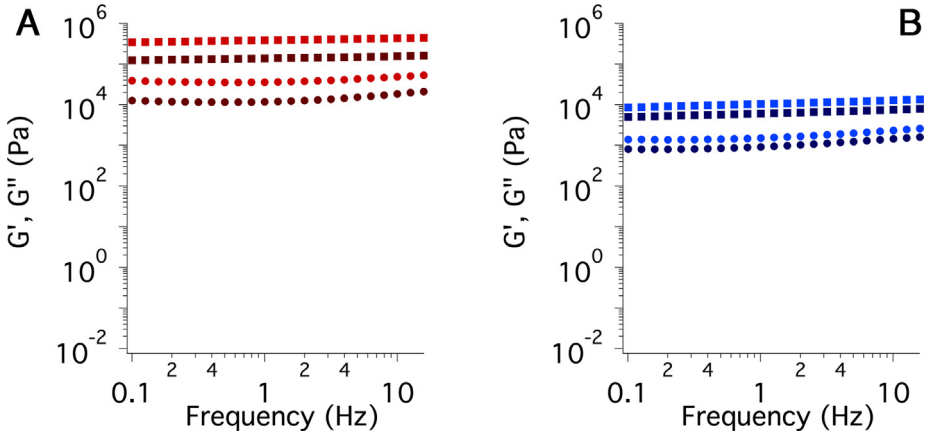

Fig. 3. Frequency sweep measurements of systems with GC and alkaline nanoparticles - G'(■), G"(●). Error bars are included in the dimensions of the markers. Measurements were repeated at least twice on duplicate samples. (A) GC-OH3 after 1 day and 7 days from the preparation (dark red and light red markers, respectively). (B) GC-CO3 after 1 day and 7 days from the preparation (dark blue and light blue markers, respectively).

SAXS measurements were used to further investigate the structure formed due to interactions between cellulose nanocrystals in the presence of ethanol and alkaline nanoparticles. Quasi-elastic light scattering (QELS), small-angle neutron scattering (SANS) and SAXS measurements are usually performed to gather information about size, shape and interparticle interactions of cellulose nanocrystals dispersions [60–66]. CNC are elongated fibrillar particles and can be modeled as cylinders, ribbons, or parallelepipeds for the analysis of scattering data. Generally, ribbons and parallelepipeds provide the most reliable fitting results [66]. In the present case, SAXS data were found to be better described by a parallelepiped form factor, implemented in the SASView software. The scattering intensity I(q) of a rectangular solid particle, having A < B < C as the three dimensions, is calculated as follows [67]:

Table 2
Tan δ (G''/G') values of GC systems with or without alkaline nanoparticles. Measurements were repeated at least twice on duplicate samples.

Systems	Tan δ 1 day	Tan δ 7 days
GC	0.17 ± 0.01	0.19 ± 0.04
GC-CO.7	0.20 ± 0.04	0.18 ± 0.01
GC-CO3	0.17 ± 0.02	0.16 ± 0.01
GC-OH.7	0.16 ± 0.01	0.09 ± 0.01
GC-OH3	0.10 ± 0.01	0.10 ± 0.01

$$I(q) = \frac{K}{V}(\Delta\rho V)^2 P(q,\sigma) + bkg$$

where K is a scale factor, V is the volume of a single particle ($V = A \times B \times C$), and the contrast term is $\Delta\rho = \rho_{CNC} - \rho_{solvent}$. $P(q,\sigma)$ is the form factor corresponding to a parallelepiped oriented at an angle given by $\cos(\sigma)$ (being σ the angle between the direction of C and the scattering vector q). The calculations are performed by using reduced lengths, instead of the actual dimensions, obtained by normalizing each length to the middle one, B, as follows:

$$a = \frac{A}{B}(< 1)$$

$$b = \frac{B}{B}(\equiv 1)$$

$$c = \frac{C}{B}(> 1)$$

The form factor, averaged over all possible orientations (spanning the whole range of $\cos(\sigma)$), is then given by the following double integral [68]:

$$P(q,\sigma) = \int_0^1 \phi_Q(\mu\sqrt{1-\sigma^2}, a)\left[S\left(\frac{\mu c\sigma}{2}\right)\right]^2 d\sigma$$

with:

$$\phi_Q(\mu, a) = \int_0^1 \left\{S\left[\frac{\mu}{2}\cos\left(\frac{\pi}{2}u\right)\right] S\left[\frac{\mu a}{2}\cos\left(\frac{\pi}{2}u\right)\right]\right\}^2 du$$

$$S(x) = \frac{\sin x}{x}$$

$$\mu = qB$$

where u is the cosine of the angle between B and the scattering vector. Fig. 5 shows the scattering curves, together with their best fitting, of the three samples analyzed, i.e., GC, GC-OH3 and GC-CO3, while fitting results are reported in Table 3.

The findings obtained from the analysis of AFM images and the information provided by the supplier suggested a length of around 130 nm for the C axis, which is outside of the experimental window of our SAXS system. Therefore, in the fitting of the SAXS data, the major C axis was constrained in the 100–150 nm range. As indicated in Table 3, an average value of about 140 nm was obtained for the analysis of the measured SAXS data. The minor length, A, was found to be 2.3–2.4 nm, in agreement with previously published data on similar systems [60,61] and with the

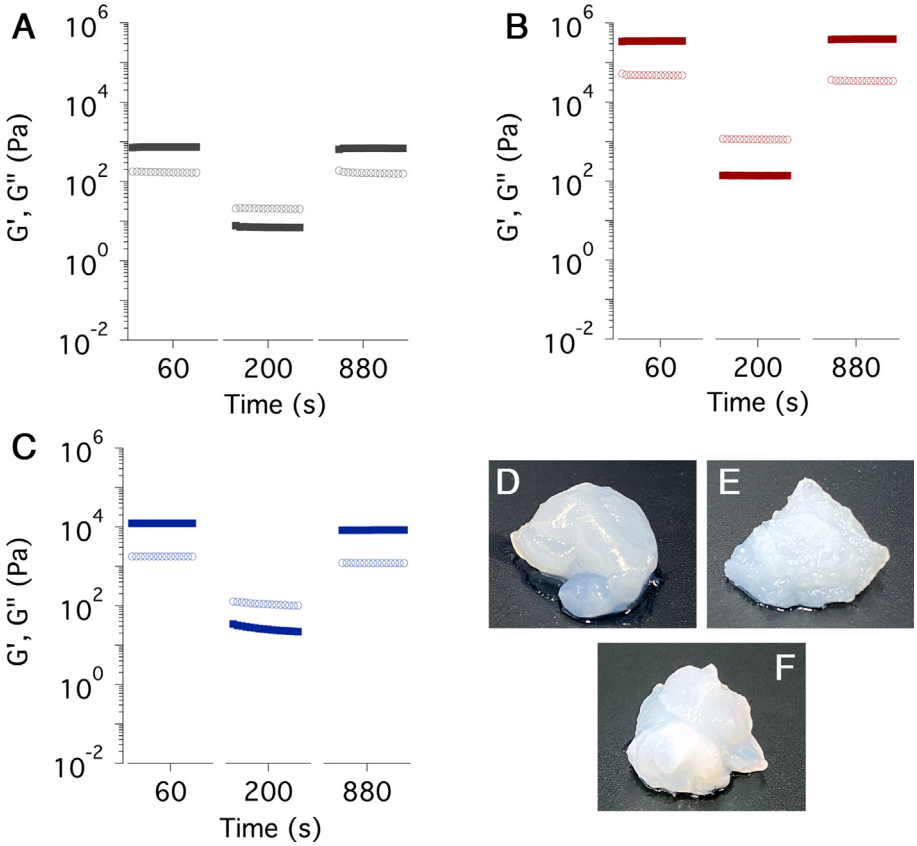

Fig. 4. Top row (right and left panels) and bottom row (left panel): three interval thixotropy tests (3ITT) of GC (A), GC-OH3 (B) and GC-CO3 (C) - G'(■), G''(○). Bottom row, right panel: visual aspect of the samples: GC (D), GC-OH3 (E) and GC-CO3 (F). Error bars are included in the dimensions of the markers. Measurements were repeated at least twice on duplicate samples.

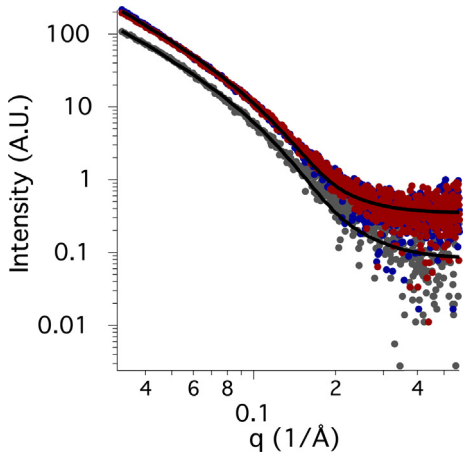

Fig. 5. SAXS curves of the three selected samples: GC, gray circles; GC-OH3, red circles; GC-CO3, blue circles. Fitting lines are represented as continuous black curves.

Table 3
Fitting parameters for the three samples analyzed. PI_A is the polydispersity index of A.

Fitting parameter	GC	GC-OH3	GC-CO3
A (Å)	23.7 ± 0.1	22.5 ± 0.1	23.9 ± 0.1
B (Å)	386.25 ± 6.7	423.9 ± 5.7	467.0 ± 6.3
C (nm)	136 ± 5	140 ± 4	138 ± 4
SLD_{CNC} (10^{-6} Å^{-2})	15.1	15.1	15.1
$SLD_{solvent}$ (10^{-6} Å^{-2})	7.6	7.6[a]	7.6[a]
PI_A	0.40 ± 0.05	0.40 ± 0.05	0.40 ± 0.05
N_{agg} (B/A)	16.3	18.9	19.5

[a] Being the volume of solubilized cations and anions in ethanol practically negligible at this concentration, the SLD of ethanol was used also for the "hybrids".

AFM results. Similar CNC, dispersed in water or in water/ethanol blend (50 wt%) have slightly higher values for A, i.e., 3.6 nm, mainly due to the different CNC hydration in these solvents compared to the neat ethanol solvent, where cellulose tends to shrink about 35% of their original size in water or water/ethanol mixtures. B axis, as previously reported by some authors [61], is significantly higher than A, and changes with the composition of the systems. This can be interpreted as if the dispersions are composed of nanocrystals clusters, rather than single particles. In fact, similarly to Uhlig et al. [61], we considered that a single particle has a square section (A × A), assuming that the interactions between GC led to the formation of plate-like ribbons having a rectangular total cross section given by A × B. Therefore, the B/A ratio can be considered the aggregation number of GC clusters. The last row of Table 3 reports the average aggregation number for the cluster of the three systems. The results show that the grafted nanocrystals' aggregation number ranges from 16 to about 19. Interestingly, the average aggregation number of GC is sensibly higher than that of CNC in water or water/ethanol (50 wt%) at the same concentration, which was found to be 9–10. This difference can be due to the combined effect of replacing water with ethanol and to the surface grafting with oleic acid, both resulting in the interparticle interaction change. Moreover, the addition of alkaline nanoparticles further increases the aggregation number.

The grafting of oleic acid, the use of ethanol as a dispersing medium, and the addition of alkaline nanoparticles act in a synergistic way increasing interactions between grafted cellulose nanocrystals, and are responsible for the increase of the clusters size, and also for the formation of macrodomains (also evidenced by AFM, see Fig. 1) responsible for the mechanical behavior assessed by rheological measurements.

3.3. Application to paper

The selected aging procedure of filter paper decreases the pH from 7.0 to 5.4, and the UTS of about 20%, as shown in Fig. 6.

The application of GC on aged paper (AP) increases the UTS to 2.4 kN/m, which is close to the value of unaged paper, showing that GC act as an effective strengthening agent. Tensile tests conducted on a control sample of paper treated with neat ethanol confirm that the increase in UTS is only due to nanocellulose. On the other hand, pH values of aged paper before and after the treatment with GC are almost the same, because nanocellulose cannot neutralize acidity. "Hybrid" systems lead to an increase in the mechanical resistance of aged filter paper. The application of GC-CO3 and GC-OH3 neutralized the present acidity and increased the pH to 8, which is considered a safe value for paper conservation. GC-OH3 induced a slightly lower increase in term of mechanical resistance, which can be ascribed to the slightly higher viscosity of the "hybrid" system, probably resulting in an irregular distribution of the particles over the paper surface. The visual aspect of paper samples was not significantly altered after treatment. In fact, the ΔE of samples treated with GC, GC-CO3, and GC-OH3 calculated with respect to AP, are 1.6, 2.5 and 2.7, respectively, close to the threshold of a color difference perceivable by the naked eye [69]. The Yellowness Index, which describes the change in color of a sample from white to yellow, was used to gather more information about the aspect of paper samples. As a result of the artificial aging, the YI increased from 4 to 22, while it was only marginally affected

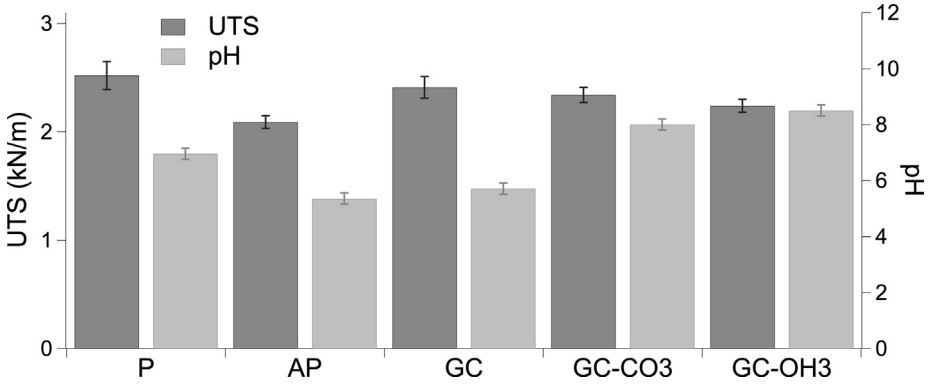

Fig. 6. Ultimate tensile strength (dark bars), and pH (light bars) of paper samples. Error bars were calculated from repeated experiments, i.e., 6 replicas for UTS and 3 replicas for pH. The beneficial effects due to the application of GC, especially in combination with alkaline nanoparticles, are clearly evidenced by the increase in UTS to values very close to unaged cellulose. Aged paper samples, AP; unaged filter paper, P; oleic acid-grafted cellulose nanocrystals dispersions, GC; GC-CO3 and GC-OH3 are the systems used for concomitant deacidification and consolidation composed of GC and calcium carbonate or calcium hydroxide nanoparticles, respectively.

by the application of GC and "hybrids" that lead to a decrease of about 2–3 units.

Therefore, the proposed "hybrid" systems are effective in concomitant strengthening and deacidification of acidic and degraded paper, without significant alterations in the original visual aspect of samples and in a fully compatible way with the original material.

4. Conclusions

Cellulose nanocrystals and alkaline nanoparticles are here proposed for the first time as a single-step deacidification and consolidation treatment for degraded cellulose-based artworks. CNC have been already used as reinforcing agents of paper before sheet formation [32,33], and alkaline nanoparticle are known to be effective for paper deacidification granting protection from degradation [12,17]. In this paper, CNC were grafted with oleic acid to obtain stable modified cellulose nanocrystal dispersions in ethanol, a solvent that can be safely used for the conservation treatment of water-sensitive works of art. Moreover, alkaline nanoparticles, obtained from a solvothermal process, can be easily mixed with the CNC to obtain the final system for cellulose-based artworks. The mechanical behavior of the studied systems have been related to the changes in the composition: interactions between cellulose nanocrystals are the driving force behind the gelation of the systems that can be either due to the surface grafting, to the use of a less polar solvent or to the introduction of cations from alkaline nanoparticles in the system. The formation of cluster of nanocellulose crystals of increased size depending on the composition of the system was shown by SAXS, confirming the results obtained from the rheological characterization. Interestingly, "hybrids" are thixotropic, a behavior particularly appealing to conservation purposes. These systems can be applied in the liquid state, or, when a more confined application is required, they can be applied in a gel-like state. The "hybrid" systems resulted highly effective in the strengthening and deacidification of acidic and degraded cellulosic material, without significant alterations in the visual aspect of samples. Future perspectives involve the grafting of nanocellulose with different fatty acids, or other chemicals, for the preparation of modified products that can be stably dispersed in apolar solvents, to preserve creased and folded paper or degraded canvas, opening new perspectives to the conservation of modern and contemporary documents and, in general, works of art realized on cellulosic support.

Acknowledgements

This work benefited from the use of the SasView application, originally developed under NSF award DMR-0520547.

Funding

This work was supported by CSGI, by China Scholarship Council (CSC) and by the European Union's Horizon 2020 research and innovation programme under grant Agreement 814496 APACHE (Active & Intelligent Packaging Materials and Display Cases as a Tool for Preventive Conservation of Cultural Heritage). SasView contains code developed with funding from the European Union's Horizon 2020 research and innovation programme under the SINE2020 project, grant agreement No 654000. MUR Prin Project 2017249YEF is also acknowledged.

Authors contribution

PB and GP conceptualized the study; QX and CR carried out the synthesis of CNC grafted derivatives; QX, GP and MB performed the physico-chemical characterization; QX studied the application to paper and aged documents; PB, QX, GP, CR and MB analyzed the data.

All authors contributed to the present text.

Declaration of Competing Interest

The authors declare no competing interests.

Data availability

All the data to reproduce these findings are either included in the manuscript or in the supplementary material.

Appendix A. Supplementary material

Supplementary data to this article can be found online at https://doi.org/10.1016/j.jcis.2020.05.018.

References

[1] J. Wouters, Coming soon to a library near you?, Science (80-) 322 (5905) (2008) 1196–1198.
[2] L. Fan, M.M. Gharpuray, Y.-H. Lee, Acid hydrolysis of cellulose, in: *Cellulose Hydrolysis*, Springer, Berlin, Heidelberg, 1987, pp. 121–148, https://doi.org/10.1007/978-3-642-72575-3_4.
[3] L. Lundgaard, W. Hansen, D. Linhjell, T. Painter, Aging of oil-impregnated paper in power transformers, Power Deliv. IEEE Trans. 19 (1) (2004) 230–239.
[4] N. Banait, W. Jencks, Reactions of anionic nucleophiles with Alpha-D-glucopyranosyl fluoride in aqueous solution through a concerted, ANDN (SN2) mechanism, J. Am. Chem. Soc. 113 (21) (1991) 7951–7958, https://doi.org/10.1021/ja00021a021.
[5] A. Conti, G. Poggi, P. Baglioni, F. De Luca, F. De Luca, On the macromolecular cellulosic network of paper: changes induced by acid hydrolysis studied by NMR diffusometry and relaxometry, Phys. Chem. Chem. Phys. 16 (18) (2014) 8409–8417, https://doi.org/10.1039/c4cp00377b.
[6] A. Conti, M. Palombo, A. Parmentier, G. Poggi, P. Baglioni, F. De Luca, Two-phase water model in the cellulose network of paper, Cellulose 24 (8) (2017) 3479–3487, https://doi.org/10.1007/s10570-017-1338-2.
[7] P. Baglioni, D. Chelazzi, R. Giorgi, G. Poggi, Colloid and materials science for the conservation of cultural heritage: cleaning, consolidation, and deacidification, Langmuir 29 (17) (2013) 5110–5122, https://doi.org/10.1021/la304456n.
[8] D. Chelazzi, R. Giorgi, P. Baglioni, Microemulsions, micelles, and functional gels: how colloids and soft matter preserve works of art, Angew. Chemie Int. Ed. 57 (25) (2018) 7296–7303, https://doi.org/10.1002/anie.201710711.
[9] M. Baglioni, J.A.L. Domingues, E. Carretti, E. Fratini, D. Chelazzi, R. Giorgi, P. Baglioni, Complex fluids confined into semi-interpenetrated chemical hydrogels for the cleaning of classic art: a rheological and SAXS study, ACS Appl. Mater. Interfaces 10 (22) (2018) 19162–19172, https://doi.org/10.1021/acsami.8b01841.
[10] M. Baglioni, Y. Jáidar Benavides, A. Desprat-Drapela, R. Giorgi, Amphiphile-based nanofludis for the removal of styrene/acrylate coatings: cleaning of stucco decoration in the uaxactun archeological site (Guatemala), J. Cult. Herit. 16 (6) (2015) 862–868, https://doi.org/10.1016/j.culher.2015.03.008.
[11] C. Mazzuca, G. Poggi, N. Bonelli, L. Micheli, P. Baglioni, A. Palleschi, Innovative chemical gels meet enzymes: a smart combination for cleaning paper artworks, J. Colloid Interface Sci. 502 (2017) 153–164, https://doi.org/10.1016/j.jcis.2017.04.088.
[12] R. Giorgi, L. Dei, M. Ceccato, C. Schettino, P. Baglioni, Nanotechnologies for conservation of cultural heritage: paper and canvas deacidification, Langmuir 18 (21) (2002) 8198–8203, https://doi.org/10.1021/la025964d.
[13] R. Giorgi, D. Chelazzi, P. Baglioni, Nanoparticles of calcium hydroxide for wood conservation. the deacidification of the vasa warship, Langmuir 21 (23) (2005) 10743–10748, https://doi.org/10.1021/la0506731.
[14] R. Giorgi, D. Chelazzi, P. Baglioni, Conservation of acid waterlogged shipwrecks: nanotechnologies for de-acidification, Appl. Phys. A Mater. Sci. Process. 83 (4) (2006) 567–571, https://doi.org/10.1007/s00339-006-3542-z.
[15] G. Poggi, N. Toccafondi, D. Chelazzi, P. Canton, R. Giorgi, P. Baglioni, Calcium hydroxide nanoparticles from solvothermal reaction for the deacidification of degraded waterlogged wood, J. Colloid Interface Sci. 473 (2016) 1–8, https://doi.org/10.1016/j.jcis.2016.03.038.
[16] R. Giorgi, D. Chelazzi, E. Fratini, S. Langer, A. Niklasson, M. Rådemar, J.-E. Svensson, P. Baglioni, Nanoparticles of calcium hydroxide for wood deacidification: decreasing the emissions of organic acid vapors in church organ environments, J. Cult. Herit. 10 (2) (2009) 206–213, https://doi.org/10.1016/j.culher.2008.06.012.
[17] G. Poggi, R. Giorgi, N. Toccafondi, V. Katzur, P. Baglioni, Hydroxide nanoparticles for deacidification and concomitant inhibition of iron-gall ink

corrosion of paper, Langmuir 26 (24) (2010) 19084–19090, https://doi.org/10.1021/la1030944.
[18] G. Poggi, N. Toccafondi, L.N. Melita, J.C. Knowles, L. Bozec, R. Giorgi, P. Baglioni, P. Baglioni, Calcium hydroxide nanoparticles for the conservation of cultural heritage: new formulations for the deacidification of cellulose-based artifacts, Appl. Phys. A 114 (3) (2014) 685–693, https://doi.org/10.1007/s00339-013-8172-7.
[19] G. Poggi, R. Giorgi, A. Mirabile, H. Xing, P. Baglioni, A stabilizer-free non-polar dispersion for the deacidification of contemporary art on paper, J. Cult. Herit. 26 (2017) 44–52, https://doi.org/10.1016/j.culher.2017.02.006.
[20] R. Giorgi, C. Bozzi, L. Dei, C. Gabbiani, B.W. Ninham, P. Baglioni, Nanoparticles of $Mg(OH)_2$: synthesis and application to paper conservation, Langmuir 21 (18) (2005) 8495–8501, https://doi.org/10.1021/la050564m.
[21] G. Poggi, M.C. Sistach, E. Marin, J.F. Garcia, R. Giorgi, P. Baglioni, Calcium hydroxide nanoparticles in hydroalcoholic gelatin solutions (GeolNan) for the deacidification and strengthening of papers containing iron gall ink, J. Cult. Herit. 18 (2016) 250–257, https://doi.org/10.1016/j.culher.2015.10.005.
[22] S. Sequeira, C. Casanova, E. Cabrita, Deacidification of paper using dispersions of Ca(OH)2 nanoparticles in isopropanol. Study of efficiency, J. Cult. Herit. 7 (4) (2006) 264–272, https://doi.org/10.1016/j.culher.2006.04.004.
[23] E. Stefanis, C. Panayiotou, Study of the photochemical stability of paper deacidified with dispersions of $Ca(OH)_2$ and $Mg(OH)_2$ nanoparticles in alcohols, Restaurator 29 (2) (2008) 125–138, https://doi.org/10.1515/rest.2008.007.
[24] S. Bastone, D.F. Chillura Martino, V. Renda, M.L. Saladino, G. Poggi, E. Caponetti, Alcoholic nanolime dispersion obtained by the insolubilisation-precipitation method and its application for the deacidification of ancient paper, Colloids Surfaces A Physicochem. Eng. Asp. 513 (2017) 241–249, https://doi.org/10.1016/j.colsurfa.2016.10.049.
[25] J.H. Stoner, R. Rushfield, Conserv. Easel Paint. (2012), https://doi.org/10.1017/CBO9781107415324.004.
[26] S. Titus, R. Schneller, E. Huhsmann, U. Hähner, G. Banik, Stabilising local areas of loss in iron gall ink copy documents from the savigny estate, Restaurator 30 (1–2) (2009) 16–50, https://doi.org/10.1515/rest.003.
[27] H.P.S. Abdul Khalil, Y. Davoudpour, M.N. Islam, A. Mustapha, K. Sudesh, R. Dungani, M. Jawaid, Production and modification of nanofibrillated cellulose using various mechanical processes: a review, Carbohydr. Polym. 99 (2014) 649–665, https://doi.org/10.1016/j.carbpol.2013.08.069.
[28] O. Nechyporchuk, M.N. Belgacem, J. Bras, Production of cellulose nanofibrils: a review of recent advances, Industr. Crops Prod. (2016) 2–25, https://doi.org/10.1016/j.indcrop.2016.02.016.
[29] S. Beck-Candanedo, M. Roman, D.G. Gray, Effect of reaction conditions on the properties and behavior of wood cellulose nanocrystal suspensions, Biomacromolecules 6 (2) (2005) 1048–1054, https://doi.org/10.1021/bm049300p.
[30] N. Lin, A. Dufresne, Physical and/or chemical compatibilization of extruded cellulose nanocrystal reinforced polystyrene nanocomposites, Macromolecules 46 (14) (2013) 5570–5583, https://doi.org/10.1021/ma4010154.
[31] Nathalie LavoineIsabelle DeslogesBertine KhelifiJulien Bras, Impact of different coating processes of microfibrillated cellulose on the mechanical and barrier properties of paper, J. Mater. Sci. 49 (7) (2014) 2879–2893, https://doi.org/10.1007/s10853-013-7995-0.
[32] I. González, M. Alcalà, G. Chinga-Carrasco, F. Vilaseca, S. Boufi, P. Mutjé, From paper to nanopaper: evolution of mechanical and physical properties, Cellulose 21 (4) (2014) 2599–2609, https://doi.org/10.1007/s10570-014-0341-0.
[33] B. Sun, Q. Hou, Z. Liu, Y. Ni, Sodium periodate oxidation of cellulose nanocrystal and its application as a paper wet strength additive, Cellulose 22 (2) (2015) 1135–1146, https://doi.org/10.1007/s10570-015-0575-5.
[34] O. Nechyporchuk, K. Kolman, A. Bridarolli, M. Odlyha, L. Bozec, M. Oriola, G. Campo-Francés, M. Persson, K. Holmberg, R. Bordes, On the potential of using nanocellulose for consolidation of painting canvases, Carbohydr. Polym. 194 (2018) 161–169, https://doi.org/10.1016/j.carbpol.2018.04.020.
[35] K. Kolman, O. Nechyporchuk, M. Persson, K. Holmberg, R. Bordes, Combined nanocellulose/nanosilica approach for multiscale consolidation of painting canvases, ACS Appl. Nano Mater. (2018), https://doi.org/10.1021/acsanm.8b00262. acsanm.8b00262.
[36] A. Bridarolli, O. Nechyporchuk, M. Odlyha, M. Oriola, R. Bordes, K. Holmberg, M. Anders, A. Chevalier, L. Bozec, Nanocellulose-based materials for the reinforcement of modern canvas-supported paintings, Stud. Conserv. 63 (sup1) (2018) 332–334, https://doi.org/10.1080/00393630.2018.1475884.
[37] L. Völkel, K. Ahn, U. Hähner, W. Gindl-Altmutter, A. Potthast, Nano meets the sheet: adhesive-free application of nanocellulosic suspensions in paper conservation, Herit Sci 5 (1) (2017), https://doi.org/10.1186/s40494-017-0134-5.
[38] M.A. Hussain, T. Liebert, T. Heinze, Acylation of cellulose with N, N′-carbonyldiimidazole-activated acids in the novel solvent dimethyl sulfoxide/tetrabutylammonium fluoride, Macromol. Rapid Commun. 25 (9) (2004) 916–920, https://doi.org/10.1002/marc.200300308.
[39] S.X. Peng, H. Chang, S. Kumar, R.J. Moon, J.P. Youngblood, A comparative guide to controlled hydrophobization of cellulose nanocrystals via surface esterification, Cellulose 23 (3) (2016) 1825–1846, https://doi.org/10.1007/s10570-016-0912-3.
[40] G. Wyszecki, W.S. Stiles, Color Science: Concepts and Methods, Quantitative Data and Formulae, second ed., John Wiley & Sons, New York, NY, 2000.
[41] ASTM E313 - 15e1. Standard Practice for Calculating Yellowness and Whiteness Indices from Instrumentally Measured Color Coordinates, 2015.
[42] ASTM D828-97. Standard Test Method for Tensile Properties of Paper and Paperboard Using Constant-Rate-of-Elongation Apparatus, 2002.
[43] TAPPI T494. Tensile Properties of Paper and Paperboard (Using Constant Rate of Elongation Apparatus), 2006.
[44] A. Casoli, C. Isca, S. De Iasio, L. Botti, S. Iannuccelli, L. Residori, D. Ruggiero, S. Sotgiu, Analytical evaluation, by GC/MS, of gelatine removal from ancient papers induced by wet cleaning: a comparison between immersion treatment and application of rigid gellan gum gel, Microchem. J. 117 (2014) 61–67, https://doi.org/10.1016/j.microc.2014.06.011.
[45] A. Casoli, P. Cremonesi, C. Isca, R. Groppetti, S. Pini, N. Senin, Evaluation of the effect of cleaning on the morphological properties of ancient paper surface, Cellulose 20 (4) (2013) 2027–2043, https://doi.org/10.1007/s10570-013-9975-6.
[46] C. Isca, L. Fuster-López, D.J. Yusá-Marco, A. Casoli, An evaluation of changes induced by wet cleaning treatments in the mechanical properties of paper artworks, Cellulose 22 (5) (2015) 3047–3062, https://doi.org/10.1007/s10570-015-0712-1.
[47] C.S.R. Freire, A.J.D. Silvestre, C.P. Neto, M.N. Belgacem, A. Gandini, Controlled heterogeneous modification of cellulose fibers with fatty acids: effect of reaction conditions on the extent of esterification and fiber properties, J. Appl. Polym. Sci. 100 (2) (2006) 1093–1102, https://doi.org/10.1002/app.23454.
[48] P. Jandura, B.V. Kokta, B. Riedl, Fibrous long-chain organic acid cellulose esters and their characterization by diffuse reflectance FTIR spectroscopy, solid-state CP/MAS13C-NMR, and X-ray diffraction, J. Appl. Polym. Sci. 78 (7) (2000) 1354–1365, https://doi.org/10.1002/1097-4628(20001114)78:7<1354::AID-APP60>3.0.CO;2-V.
[49] N. Johar, I. Ahmad, A. Dufresne, Extraction, preparation and characterization of cellulose fibres and nanocrystals from rice husk, Ind. Crop. Prod. 37 (1) (2012) 93–99, https://doi.org/10.1016/j.indcrop.2011.12.016.
[50] Simon B. Ross-Murphy, Structure–property relationships in food biopolymer gels and solutions, J. Rheol. 39 (6) (1995) 1451–1463, https://doi.org/10.1122/1.550610.
[51] T. Phan-Xuan, A. Thuresson, M. Skepö, A. Labrador, R. Bordes, A. Matic, Aggregation behavior of aqueous cellulose nanocrystals: the effect of inorganic salts, Cellulose 23 (6) (2016) 3653–3663, https://doi.org/10.1007/s10570-016-1080-1.
[52] H. Dong, J.F. Snyder, K.S. Williams, J.W. Andzelm, Cation-induced hydrogels of cellulose nanofibrils with tunable moduli, Biomacromolecules 14 (9) (2013) 3338–3345, https://doi.org/10.1021/bm400993f.
[53] M. Chau, S.E. Sriskandha, D. Pichugin, H. Thérien-Aubin, D. Nykypanchuk, G. Chauve, M. Méthot, J. Bouchard, O. Gang, E. Kumacheva, Ion-mediated gelation of aqueous suspensions of cellulose nanocrystals, Biomacromolecules 16 (8) (2015) 2455–2462, https://doi.org/10.1021/acs.biomac.5b00701.
[54] I.S. Chronakis, L. Piculell, J. Borgstriim, Rheology of kappa-carrageenan in mixtures of sodium and cesium iodide : two types of gels, Carbohydr. Polym. 31 (4) (1996) 215–225.
[55] S. Ikeda, K. Nishinari, "Weak Gel "-type rheological properties of aqueous dispersions of nonaggregated K -carrageenan helices, J. Agric. Food Chem. 49 (9) (2001) 4436–4441, https://doi.org/10.1021/jf0103065.
[56] J. Mewis, N.J. Wagner, Thixotropy, Adv. Colloid Interface Sci. 147–148 (2009) 214–227, https://doi.org/10.1016/j.cis.2008.09.005.
[57] O.S. Toker, S. Karasu, M.T. Yilmaz, S. Karaman, Three Interval Thixotropy Test (3ITT) in food applications: a novel technique to determine structural regeneration of mayonnaise under different shear conditions, Food Res. Int. 70 (2015) 125–133, https://doi.org/10.1016/j.foodres.2015.02.002.
[58] M.T. Yilmaz, C. Vatansever, Three interval thixotropy test to determine structural regeneration of a glucomannan based hydrocolloid film at air/water interface: interfacial, molecular, thermal and surface characterization, Food Hydrocoll. 61 (2016) 458–468, https://doi.org/10.1016/j.foodhyd.2016.06.004.
[59] H.A. Barnes, Thixotropy - a review, J. Nonnewton. Fluid Mech. 70 (1–2) (1997) 1–33, https://doi.org/10.1016/S0377-0257(97)00004-9.
[60] Y. Mao, K. Liu, C. Zhan, L. Geng, B. Chu, B.S. Hsiao, Characterization of nanocellulose using small-angle neutron, X-ray, and dynamic light scattering techniques, J. Phys. Chem. B 121 (6) (2017) 1340–1351, https://doi.org/10.1021/acs.jpcb.6b11425.
[61] M. Uhlig, A. Fall, S. Wellert, M. Lehmann, S. Prévost, L. Wågberg, R. von Klitzing, G. Nyström, Two-dimensional aggregation and semidilute ordering in cellulose nanocrystals, Langmuir 32 (2) (2016) 442–450, https://doi.org/10.1021/acs.langmuir.5b04008.
[62] C. Bonini, L. Heux, J.-Y. Cavaillé, P. Lindner, C. Dewhurst, P. Terech, Rodlike cellulose whiskers coated with surfactant: a small-angle neutron scattering characterization, Langmuir 18 (8) (2002) 3311–3314, https://doi.org/10.1021/la015511t.
[63] C. Schütz, M. Agthe, A.B. Fall, K. Gordeyeva, V. Guccini, M. Salajková, T.S. Plivelic, J.P.F. Lagerwall, G. Salazar-Alvarez, L. Bergström, Rod packing in chiral nematic cellulose nanocrystal dispersions studied by small-angle X-ray scattering and laser diffraction, Langmuir 31 (23) (2015) 6507–6513, https://doi.org/10.1021/acs.langmuir.5b00924.
[64] F. Cherhal, F. Cousin, I. Capron, Influence of charge density and ionic strength on the aggregation process of cellulose nanocrystals in aqueous suspension, as revealed by small-angle neutron scattering, Langmuir 31 (20) (2015) 5596–5602, https://doi.org/10.1021/acs.langmuir.5b00851.
[65] Y. Su, C. Burger, H. Ma, B. Chu, B.S. Hsiao, Exploring the nature of cellulose microfibrils, Biomacromolecules 16 (4) (2015) 1201–1209, https://doi.org/10.1021/bm501897z.

[66] Y. Su, C. Burger, B.S. Hsiao, B. Chu, Characterization of TEMPO-oxidized cellulose nanofibers in aqueous suspension by small-angle X-ray scattering, J. Appl. Crystallogr. 47 (2) (2014) 788–798, https://doi.org/10.1107/S1600576714005020.
[67] S.R. Kline, Reduction and analysis of SANS and USANS data using IGOR Pro, J. Appl. Crystallogr. 39 (6) (2006) 895–900, https://doi.org/10.1107/S0021889806035059.
[68] P. Mittelbach, G. Porod, Small-angle X-ray scattering by dilute colloid sytems. the calculation of scattering curves for parallelepipeds, Acta Phys. Austriaca 14 (1961) 185–211.
[69] R.F. Witzel, R.W. Burnham, J.W. Onley, Threshold and suprathreshold perceptual color differences, J. Opt. Soc. Am. 63 (5) (1973) 615, https://doi.org/10.1364/JOSA.63.000615.